Influence of electron-boundary scattering on thermoreflectance calculations after intra- and interband transitions induced by short-pulsed laser absorption

Patrick E. Hopkins*
Engineering Sciences Center, Sandia National Laboratories, Albuquerque, New Mexico 87185-0346, USA
(Received 4 September 2009; revised manuscript received 8 December 2009; published 12 January 2010)

Ultrashort pulsed lasers are effective tools for use in a wide array of nanoscale applications, ranging from precise machining of nanomaterials, to deposition of nanocomposites, to diagnostics for observations of transport properties on atomistic time and length scales. One critical caveat of these applications is predicting and controlling the temperature of the materials after the absorbed laser pulse. At relatively low absorbed laser powers, the temperature can be determined from the reflected energy from the laser pulse off the sample surface as the reflectivity and the temperature change are linearly related. However, as laser pulses become more powerful, thereby inducing large temperature changes, and as materials continue to decrease in characteristic lengths, thereby causing substrate interference affecting the absorbed energy, the determination of the temperature from reflectance becomes more complicated than the traditionally assumed linear relation. In this work, a reflectance model is developed that accounts for large temperature fluctuations in thin-film metals by utilizing the temperature dependencies of the intraband ("free" electron) and interband ("bound" electron) dielectric functions and multiple reflection theory. Electron-electron, electron-phonon, and electron-substrate scattering are exploited and the change in reflectance as a function of these various scattering events is studied in the case of both intra- and interband excitations. This thermoreflectance model is compared to thermoreflectance data on thin Au films.

DOI: 10.1103/PhysRevB.81.035413 PACS number(s): 78.20.N−, 78.20.Ci, 78.20.Bh, 63.20.kd

I. INTRODUCTION

Electron-interface scattering is a critical transport mechanism in the development and design of nanocomposites and devices, the engineering importance ever increasing as material and device sizes continue to decrease to atomistic limits. This interface scattering pathway creates an additional form of thermal resistance. Accurate measurements and understanding of electron-interface thermal resistance can lead to the control and manipulation of this thermal process, which has major implications in the further development of applications to enhance or restrict thermal transport on the nanoscale, such as chip-level cooling or thermoelectric refrigeration, respectively.[1]

Time-domain short-pulsed thermoreflectance spectroscopy is a robust technique that has been used by several groups to back out various electronic thermal processes in nanomaterials, including electron-gas Fermi relaxation,[2–4] electron-phonon (ep) energy transfer,[5–11] recombinatory processes in semiconductors,[4,12,13] and electron-electron (ee) thermal conductance.[14,15] However, with decreasing characteristic lengths of nanodevices and increasing power demands, difficulties in determining these aforementioned thermal phenomena arise since the time and length scales associated with these phenomena converge. For example, Hopkins *et al.*[8] measured the electron-phonon coupling factor, G, of thin Au films in the free-electron limit (no interband excitations). However, due the electron-interface scattering, determining G was not as simple as the traditional analysis of fitting the two-temperature model[16] to the experimental data.[17]

In the situation where multiple thermal phenomena are occurring on similar scales during thermoreflectance measurements, the measured change in reflectance is affected due to the various scattering mechanisms. The basis for quantifying the various scattering processes is then related to the change in reflectance through the electronic temperature change, which is then related to some type of thermal model that relates temperature change to the electronic scattering rate. The key, therefore, is an accurate thermoreflectance model that can relate multiple electronic-scattering processes to the change in reflectance as a function of temperature.

Rosei[18] developed a thermoreflectance model to account for the large change in reflectance around interband transition thresholds observed in several experimental studies.[19–23] Hohlfeld *et al.*[24,25] extended Rosei's work by fitting a modified thermoreflectance model to experimental data to scattering times in materials. Smith and Norris[26] derived a thermoreflectance model for intraband transitions in Au that specifically accounted for electron-electron and electron-phonon scattering. Recently, Hopkins[27] extended Smith and Norris' model to thin films, taking into account multiple reflections off interfaces, and included an electron-interface scattering term to relate the thermoreflectance signal to the electron-interface thermal processes.

In this paper, a thermoreflectance model is derived that accounts for both intra- and interband transitions and includes an electron-interface scattering term. The model takes into account specific Fermi-level transitions observed in measured optical properties of bulk materials, of which there is a wealth of tabulated data.[28–32] In the next section, the thermoreflectance model is derived for a thin film on a substrate. In Sec. III, the thermoreflectance signal is calculated for Au in the intra- and interband transition regimes. The effects of electron-electron and electron-phonon scattering are discussed. In Sec. IV, an electron-interface scattering term is introduced and the effects of this scattering mechanism on thermoreflectance at intra- and interband energies in

 ©2010 The American Physical Society

Au are examined. Although example calculations are shown for Au in this work, the model presented in this paper is easily applicable to any metal.[33]

II. REFLECTANCE IN THIN FILMS

A thermoreflectance signal is a change in the baseline reflectivity of a sample surface resulting from a change in temperature of the sample. The reflectivity of a bulk material (film) at the air (vacuum)/film interface is given by

$$R=\frac{(n_1-1)^2+n_2^2}{(n_1+1)^2+n_2^2}, \tag{1}$$

where n_1 and n_2 are the real (refractive index) and imaginary (extinction coefficient) parts of the complex index of refraction, $\hat{n}$. However, in thin films on the order of the optical penetration depth, reflection and absorption at the film/substrate interface can cause a change in the measured reflectivity of the sample surface due to multiple reflections propagating in the film. From thin-film optics, the reflectivity of a thin film on a substrate, where the incident medium is air, is given by[34]

$$R_f = r^* r, \tag{2}$$

where

$$r=\frac{(m_{11}+\hat{n}_s m_{12})-(m_{21}+\hat{n}_s m_{22})}{(m_{11}+\hat{n}_s m_{12})+(m_{21}+\hat{n}_s m_{22})} \tag{3}$$

with $\hat{n}_s$ being the complex index of refraction of the substrate and r^* is the complex conjugate of Eq. (3). In Eq. (3), $m_{i,j}$ are the components of the characteristic thin-film matrix,[35] defined as

$$M=\begin{bmatrix} \cos\delta & -\dfrac{i}{\hat{n}_f}\sin\delta \\ -i\hat{n}_f\sin\delta & \cos\delta \end{bmatrix}, \tag{4}$$

where $\delta=\omega L\hat{n}_1/c$ and ω is the angular frequency of the radiation, L is the film thickness, and c is the speed of light.

The key to determining Eq. (4) is knowledge of n_1 and n_2 for the film and substrate. Since this work focuses on thermoreflectance due to temperature modulations in the film, an analytical model is used to determine n_1 and n_2 in order to exploit the temperature dependence of the film's optical properties yet tabulated values will be used for the substrate optical properties since only small, negligible temperature changes are assumed in the substrate. The refractive index and extinction coefficient are related to the complex optical dielectric function, $\hat{\varepsilon}=\varepsilon_1+i\varepsilon_2$, through[33]

$$n_1=\frac{1}{\sqrt{2}}[(\varepsilon_1^2+\varepsilon_2^2)^{1/2}+\varepsilon_1]^{1/2} \tag{5}$$

and

$$n_2=\frac{1}{\sqrt{2}}[(\varepsilon_1^2+\varepsilon_2^2)^{1/2}-\varepsilon_1]^{1/2}. \tag{6}$$

Now the complex dielectric function can also be expressed as $\hat{\varepsilon}=\hat{\varepsilon}_{\text{intra}}+\hat{\varepsilon}_{\text{inter}}$, which explicitly separates the contributions due to intraband transitions (free electrons) and interband transitions (bound electrons).

The intraband part, $\hat{\varepsilon}_{\text{intra}}$, is described by the well-known Drude model, given by

$$\hat{\varepsilon}_{\text{intra}}=1-\frac{\omega_p^2}{\omega(\omega+i\tau_f^{-1})}, \tag{7}$$

where ω_p is the plasma angular frequency of the film, ω is the angular frequency of the absorbed radiation ($\omega=2\pi c/\lambda$, where c is the speed of light and λ is the wavelength of the wavelength of the absorbed radiation), and τ_f^{-1} is the scattering rate of the free electrons undergoing intraband transitions.

The interband part of the complex dielectric function, $\hat{\varepsilon}_{\text{inter}}$, is given by a model based on the solution to the Liouville equation for the one-electron density matrix in first-order perturbation theory developed by Jha and Warke[36] and addressed in more detail by Rustagi,[37] given by

$$\hat{\varepsilon}_{\text{inter},j}=-\frac{4\pi e^2}{m^2\omega^2}\sum_{k=k_F}^{k_0}\frac{\langle p_j\rangle^2}{E_{k,j}}\left[\frac{\hbar\omega+i\hbar\tau_j^{-1}}{E_{k,j}-\hbar\omega-i\hbar\tau_j^{-1}} - \frac{\hbar\omega+i\hbar\tau_j^{-1}}{E_{k,m}+\hbar\omega+i\hbar\tau_j^{-1}}\right], \tag{8}$$

where e is the electron charge, m is the effective mass of the electrons (which, in Au, electrons excited to the Fermi surface have effective masses that are nearly the free-electron mass, so in this work, the free-electron mass is assumed), k_0 is the radius of the Brillouin zone, k_F is the radius of the Fermi surface given by $k_F=\sqrt{2mE_F}/\hbar$ with E_F being the Fermi energy, τ_j^{-1} is the scattering rate of the electrons that are excited via some interband transition from j, and $\langle p_j\rangle$ is the transition momentum matrix element for transition j. Assuming an isotropic dispersion of a parabolic conduction band and a flat d band, and assuming transitions between the d band and conduction band yields the potential energy of the conduction band with respect to the d-band transition edge as $E_{k,j}=E_j+\hbar^2k^2/(2m)$, where E_j is the energy gap between the conduction and d band in the center of the Brillouin zone. With this approximation, $\langle p_j\rangle^2=mE_{p,j}/2$, where $E_{p,j}$ is a constant. Converting Eq. (8) to an integration yields

$$\hat{\varepsilon}_{\text{inter},j}=\frac{3}{2}\frac{\omega_p^2}{\omega^2}\frac{E_{p,j}}{E_F}\frac{1}{k_F}\int_{k_F}^{k_0}\left(\frac{z_1^2}{k^2-z_1^2}-\frac{z_1'^2}{k^2-z_1'^2}-\frac{2z_0^2}{k^2-z_0^2}\right)dk, \tag{9}$$

where $k_0=2^{1/3}k_F$,[38]

$$z_{n,j}^2=\frac{2m}{\hbar^2}(n\hbar\omega+in\hbar\tau_j^{-1}-E_j) \tag{10}$$

and

$$z_{n,j}'^2=\frac{2m}{\hbar^2}(n\hbar\omega+in\hbar\tau_j^{-1}+E_j). \tag{11}$$

In Au, the lowest energy d band to Fermi-surface transition at 516 nm (2.4 eV) affects the reflectance spectra drastically more than other Fermi-surface transitions in the wavelength

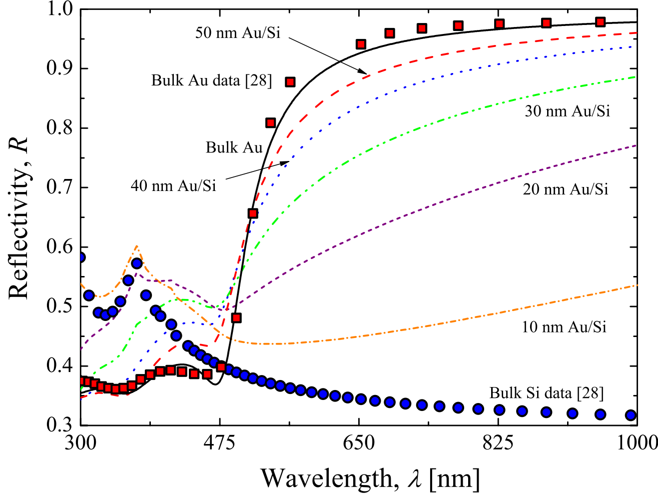

FIG. 1. (Color online) Reflectivity data as a function of wavelength of bulk Au (red squares) and bulk Si (blue circles) along with calculations for the reflectivity as a function of wavelength for bulk Au (solid line) using the reflectivity model discussed in Sec. II. The dotted and dashed lines show reflectivity calculations of Au films of various thicknesses on a bulk Si substrate using the reflectivity model taking into account reflections from the Au/Si interface via Eq. (2).

range of interest in this study ($\lambda \leq 300-1000$ nm or 1.24–4.13 eV). However, there are other Fermi-surface transitions in this wavelength range that do affect reflectance near the 2.4 eV transition as apparent by the shape of the Au reflectivity at 300 K plotted in Fig. 1. Each inflection point in the reflectance spectra roughly corresponds to an interband Fermi-surface transition.[33,39] These transitions appear as local extrema in the thermoderivative of $\hat{\varepsilon}_2$.[18,39] Therefore, for every inflection point in the reflectivity of Au, a new transition must be considered in the interband dielectric function via Eq. (9). Three Fermi-surface transitions affect the reflectance in the wavelength range of interest in this study, so the interband dielectric function is given by $\hat{\varepsilon}_{\text{inter}}=\sum_{j=1}^{3}\hat{\varepsilon}_{\text{inter},j}$.

The sum of Eqs. (7) and (9) gives $\hat{\varepsilon}=\hat{\varepsilon}_{\text{intra}}+\hat{\varepsilon}_{\text{inter}}$ which is related to Eqs. (5) and (6) by $\hat{\varepsilon}=\varepsilon_1+i\varepsilon_2$. To determine the interband dielectric function in Au at 300 K, n_1 and n_2 were calculated and best fit with tabulated data[29] iterating ω_p, τ_f^{-1}, and $E_{p,j}$, E_j, and τ_j^{-1} for each of the three transitions. The best-fit values used to calculate the complex dielectric function in Au listed in Table I. The plasma frequency fitted result, $\omega_p=1.3\times10^{16}$ rad s^{-1}, is in excellent agreement with literature values of the plasma frequency, $1.3-1.4\times10^{16}$ rad s^{-1}.[28,30] As seen in Fig. 1, the calculation of R for bulk Au agrees well with R determined from the tabulated data on bulk Au.[29] Using Eq. (2), the reflectance for thin Au films on Si at 300 K are also shown in Fig. 1 for film thicknesses of 10, 20, 30, 40, and 50 nm. Also shown is the bulk reflectivity of Si at 300 K calculated from the tabulated values of n_1 and n_2 (Ref. 29) used to calculate the thin-film Au on Si reflectivity.

III. THERMOREFLECTANCE IN INSULATED THIN FILMS

To determine the thermoreflectance signal, or the change in reflectance due to a temperature change, the temperature dependency of the complex dielectric function must be known. This is determined through the electron-scattering rates. In bulk, clean metals, the primary scattering mechanisms of the free electrons at the Fermi surface are ee and ep scattering. Therefore, employing Matthiessen's Rule, $\tau_f^{-1}=\tau_{\text{ee}}^{-1}+\tau_{\text{ep}}^{-1}$. The electron-electron and electron-phonon scattering times are given by $\tau_{\text{ee}}^{-1}=AT_e^2$ and $\tau_{\text{ep}}^{-1}=BT_p$, respectively, where A and B are scattering coefficients that are typically determined by resistivity experiments[40] and T_e and T_p are the electron and phonon system temperatures. Literature values of A and B in Au are 1.2×10^7 K^{-2} s^{-1} and 1.23×10^{11} K^{-1} s^{-1},[41] respectively, yielding $\tau_f^{-1}=3.8\times10^{13}$ s^{-1} when the electrons and phonons are at 300 K, in good agreement with the value for τ_f^{-1} determined from the complex dielectric function fit to data at 300 K, 2.0×10^{13} s^{-1}. In this work, electron temperatures from 300–3000 K are considered which ensures no d-band excitations due to Fermi smearing in Au.[42] In this temperature regime, Au has a constant electron-phonon coupling constant,[42] so A is taken as the literature value for electron-electron scattering of free electrons and B is determined from $\tau_f^{-1}=\tau_{\text{ee}}^{-1}+\tau_{\text{ep}}^{-1}$ at 300 K using the fitted value for τ_f^{-1}, which yields $B=6.3\times10^{10}$ K^{-1} s^{-1}. Note that the electron-electron and electron-phonon scattering constants are relatively temperature independent in Au.[40] Therefore, the electron temperature dependency of the intraband dielectric function takes a T_e^2 dependence.[26] The temperature dependency of the interband dielectric function follows the temperature dependency of the Fermi energy described by the Sommerfeld expansion.[43] The electron-scattering rates in the interband dielectric function are assumed temperature independent, so the τ_j^{-1} constants in Eq. (9) are treated as dampening coefficients, similar to those in the Lorentz model for oscillators.[33] For this

TABLE I. Parameters used in reflectance model discussed in Sec. II.

Parameter	B	ω_p	τ_f^{-1}	$E_{p,1}$	E_1	τ_1^{-1}
Units	10^{10} K^{-1} s^{-1}	10^{16} rad s^{-1}	10^{14} s^{-1}	eV	eV	10^{14} s^{-1}
Value used in model	6.3	1.3	0.20	1.5	−2.9	2.0
Parameter	$E_{p,2}$	E_2	τ_2^{-1}	$E_{p,3}$	E_3	τ_3^{-1}
Units	eV	eV	10^{14} s^{-1}	eV	eV	10^{14} s^{-1}
Value used in model	1.5	−2.0	4.0	5.0	−1.0	7.0

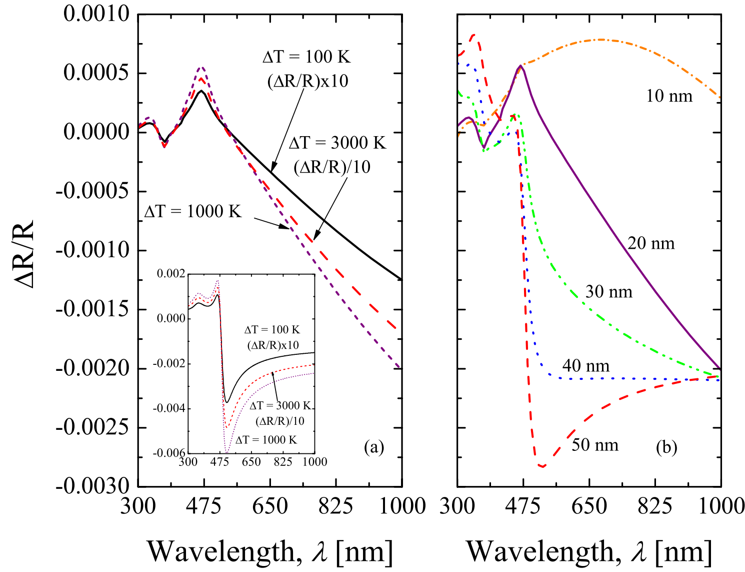

FIG. 2. (Color online) (a) Thermoreflectance signal on a 20 nm Au film on a bulk Si substrate for three different changes in electron temperatures. The inset shows the thermoreflectance signal for bulk Au for the same three changes in electron temperature. (b) Thermoreflectance signal of Au film of various thicknesses on a Si substrate.

study, a constant phonon temperature of 300 K is assumed which is a valid assumption for thermoreflectance studies using short pulses where the electron system rapidly changes temperature from pulse absorption before any substantial energy is transferred to the lattice. By calculating the complex dielectric function at various electron temperatures, the thermoreflectance signal, $\Delta R/R$, is calculated via

$$\frac{\Delta R(\Delta T_e)}{R} = \frac{R(T_e) - R(300\ \mathrm{K})}{R(300\ \mathrm{K})}. \qquad (12)$$

Figure 2 shows thermoreflectance calculations for thin Au films on Si substrates. Figure 2(a) shows the thermoreflectance signal on a 20 nm Au film for three different changes in temperatures. The inset of Fig. 2(a) shows the thermoreflectance signal for bulk Au for the same three changes in temperature. The signals are drastically different. Figure 2(b) shows how the thermoreflectance signal of an Au film on a Si substrate changes with film thickness. Even at Au film thickness of 50 nm, the thermoreflectance signal is still affected by the underlying substrate. In addition, the thermoreflectance signal is affected by the underlying signal differently at different photon energies, which will be addressed in more detail in the next section.

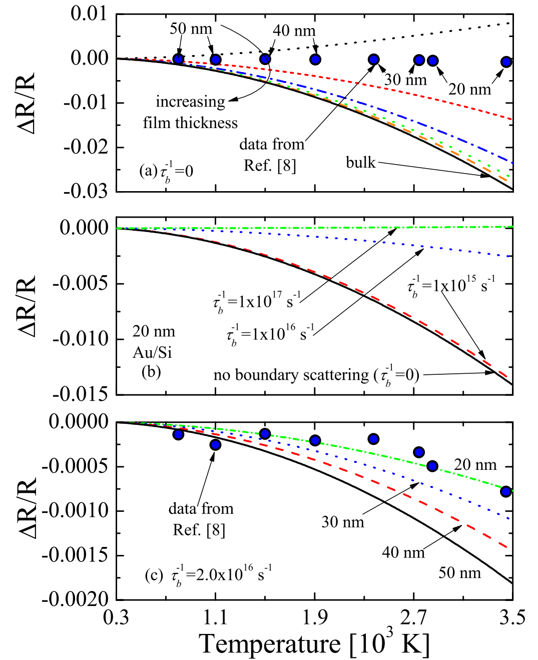

FIG. 3. (Color online) (a) 800 nm thermoreflectance signal for Au films of varying thickness on a Si substrate assuming an insulated (τ_b=0) Au/Si interface along with experimental thermoreflectance data taking at 800 nm for thin Au films (film thicknesses are 20, 30, 40, and 50 nm) on Si substrates (Ref. 8). The predicted thermoreflectance signal of Au/Si at 800 nm assuming no electron-boundary scattering is much greater (absolute value) than the measured data, to the point where the measured data appear approximately zero compared to the predictions. (b) Calculations for $\Delta R/R$ with varying values for τ_b^{-1}. As τ_b^{-1} increases, the magnitude of the 800 nm thermoreflectance signal for 20 nm Au/Si decreases. (c) $\Delta R/R$ for different Au film thicknesses for Au/Si compared to the data from Hopkins *et al.* (Ref. 8) assuming $\tau_b^{-1}=2.0\times10^{16}$ s^{-1}. Taking into account electron-boundary scattering drastically improves the predictions of $\Delta R/R$.

IV. EFFECTS OF ELECTRON-BOUNDARY SCATTERING ON THERMOREFLECTANCE (NONINSULATED THIN FILMS)

When the film thickness is less than the thermal penetration depth in the material, electron-boundary scattering can affect the thermoreflectance signal.[27] This arises due to another scattering mechanism for the free electrons. In the case of electron-boundary scattering, the electron relaxation time of the free electrons is given by $\tau_f^{-1}=\tau_{ee}^{-1}+\tau_{ep}^{-1}+\tau_b^{-1}$, where τ_b^{-1} is the electron-boundary scattering rate. In this case, the di-

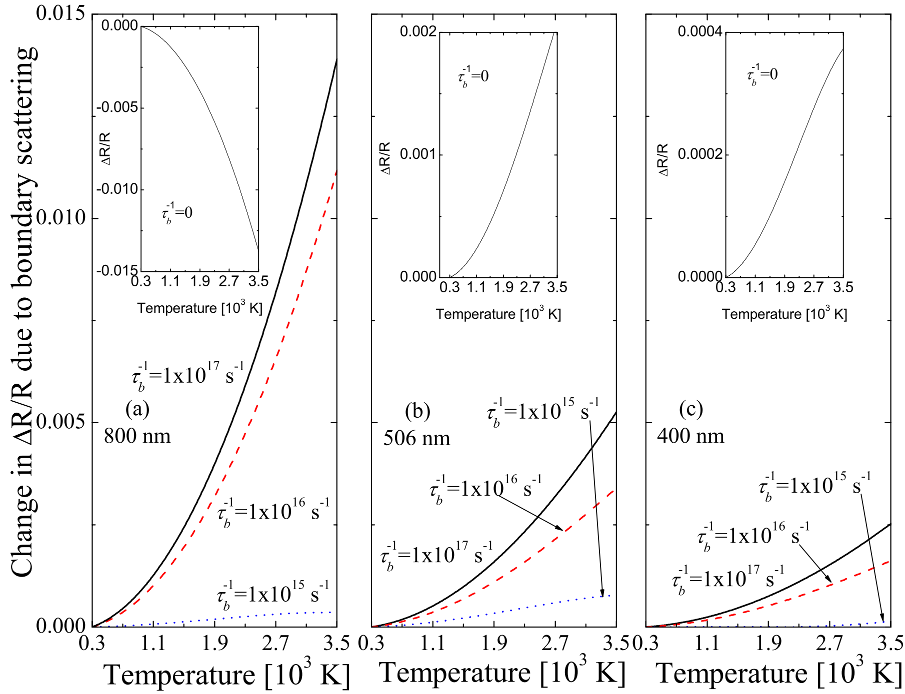

FIG. 4. (Color online) Change in the thermoreflectance signal as a function of temperature for different electron-boundary scattering rates at three different wavelengths—(a) 800 nm; (b) 506 nm; and (c) 400 nm—for a 20 nm Au film on a Si substrate. The values shown are the changes in the thermoreflectance signal due to electron-boundary scattering for a 20 nm Au film—the absolute values of the difference between $\Delta R/R$ using τ_b^{-1} listed in the figure and $\Delta R/R$ when $\tau_b^{-1}=0$—this is effectively showing the sensitivity of the thermoreflectance signal to τ_b^{-1}. Comparing the thermoreflectance signal at the varying wavelengths shows that at high temperatures, $\Delta R/R$ is nearly 3–4 times greater when probing at 800 nm than when probing interband transitions for τ_b^{-1} expected in thin Au films [i.e., on the order of 10^{16} s^{-1} (Ref. 27)]. The insets show the thermoreflectance signals as a function of temperature for a 20 nm Au film assuming $\tau_b^{-1}=0$ for the different wavelengths.

electric function is affected, which changes the thermoreflectance signal due to the additional scattering mechanism.

The thermoreflectance signal at 800 nm for Au/Si as a function of electron temperature is shown in Fig. 3. Figure 3(a) shows the 800 nm thermoreflectance signal for Au films of varying thickness on a Si substrate assuming an insulated ($\tau_b=0$) Au/Si interface. Also shown in this figure are experimental thermoreflectance data taken at 800 nm for thin Au films (with varying thicknesses of 20, 30, 40, and 50 nm) on Si substrates as a function of electron temperature.[8] The predicted thermoreflectance signal of Au/Si at 800 nm assuming no electron-boundary scattering is much greater (absolute value) than the measured data, to the point where the measured data appear approximately zero compared to the predictions. This can be explained by the change in thermoreflectance due to electron-boundary scattering. The effect of boundary scattering on the thermoreflectance signal of a 20 nm Au film on a Si substrate is shown in Fig. 3(b), which shows calculations for $\Delta R/R$ with varying values for τ_b^{-1}. As τ_b^{-1} increases, the magnitude of the 800 nm thermoreflectance signal for 20 nm Au/Si decreases. The expression developed by Hopkins[27] for electron-boundary scattering during an electron-phonon nonequilibrium predicts a boundary scattering rate of $\sim 2.0\times 10^{16}$ s^{-1}. Using $\tau_b^{-1}=2.0\times 10^{16}$ s^{-1}, Fig. 3(c) shows $\Delta R/R$ as a function of Au film thickness for Au/Si compared to the data from Hopkins *et al.*[8] Taking into account electron-boundary scattering drastically improves the predictions of $\Delta R/R$.

Although this effect was observed experimentally at 800 nm, Hohlfeld *et al.*[7] conducted a similar study to Hopkins *et al.* differing only by measuring thermoreflectance signals causing interband transitions (using 500 and 540 nm probe wavelengths) and did not observe the effects of electron-boundary scattering in their measurements of electron-phonon coupling factor in Au. Potential reasons why Hohlfeld *et al.*'s work did not observe boundary scattering phenomena lie in the thermoreflectance model. First and foremost, the interband thermoreflectance model used in Hohlfeld *et al.*'s analysis[24] did not take into account reflections from the film/substrate interface, i.e., it was not thickness dependent. As seen from the thickness-dependent thermoreflectance model derived in this work, for Au/Si, these substrate reflections drastically affect the thermoreflectance signal.

Another potential reason for the discrepancy is the sensitivity of the thermoreflectance model to electron-boundary scattering at different wavelengths (as previously mentioned, Hohlfeld *et al.*[7] used thermoreflectance signals at 500 and 546 nm to determine the electron-phonon coupling factor in Au). Figure 4 shows the change in the thermoreflectance signal as a function of temperature for different electron-boundary scattering rates at three different wavelengths—(a) 800 nm; (b) 506 nm; and (c) 400 nm—for a 20 nm Au film on a Si substrate. The values shown in Fig. 4 are the changes in the thermoreflectance signal due to electron-boundary scattering for a 20 nm Au film—the absolute values of the

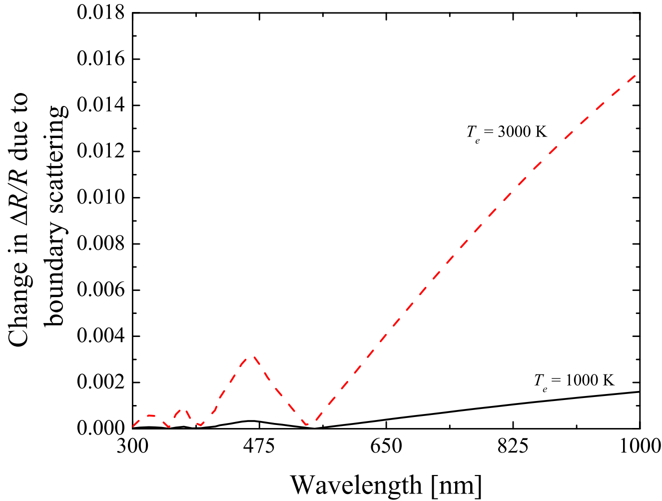

FIG. 5. (Color online) Sensitivity of the 20 nm Au/Si thermoreflectance signal to electron-boundary scattering as a function of wavelength for two different electron temperatures, 1000 and 3000 K. The thermoreflectance signal of Au is much more sensitive to electron-boundary scattering in the free-electron regime.

difference between $\Delta R/R$ using τ_b^{-1} listed in the figure and $\Delta R/R$ when $\tau_b^{-1}=0$—this is effectively showing the sensitivity of the thermoreflectance signal to τ_b^{-1}. Comparing the thermoreflectance signal at the varying wavelengths shows that at high temperatures, $\Delta R/R$ is nearly 3–4 times greater when probing at 800 nm than when probing interband transitions for τ_b^{-1} expected in thin Au films (i.e., on the order of 10^{16} s^{-1}).[27] The insets show the thermoreflectance signals as a function of temperature for a 20 nm Au film assuming $\tau_b^{-1}=0$ for the different wavelengths.

Figure 5 shows the sensitivity of the 20 nm Au/Si thermoreflectance signal to electron-boundary scattering as a function of wavelength for two different electron temperatures, 1000 and 3000 K. The thermoreflectance signal of Au is much more sensitive to electron-boundary scattering in the free-electron regime. This offers another explanation for the difference between the electron-phonon coupling results reported by Hohlfeld *et al.*—who probed the Au response around wavelengths in which the interband thermoreflectance response would dominate that from the free electrons—and Hopkins *et al.*—who probed the Au response in the free-electron regime. Figure 5 clearly shows that the thermoreflectance signal from interband transitions in Au is much stronger than the thermoreflectance signal due to electron-boundary scattering at wavelengths close to and lower than the interband transition threshold. However, in the free-electron regime, the interband response plays a minor role in the thermoreflectance signal so that free-electron scattering phenomena, such as electron-boundary scattering, can be clearly observed.

The model developed in this work shows the effects of boundary scattering on the thermoreflectance response of a thin metal film on a dielectric substrate. This model is generalized to account for any metal film or substrate given experimentally determined values for the complex index of refraction of the corresponding bulk material. For example, the change in the thermoreflectance response due to structural or chemical alterations of the substrate material can easily be accounted for if the optical properties of the altered substrate are known. In addition, this model assumes a constant rate for electron-boundary scattering. A temperature-dependent boundary scattering rate is easily incorporated, although the material comprising the boundary and intrinsic properties of the boundary can drastically affect the temperature dependency and scattering rates.[27,44–46] Although this work considers boundary scattering as a temperature-independent constant, examination of Fig. 4 shows that the trends in the thermoreflectance responses for the different wavelengths are similar regardless of the electron-boundary scattering constant; that is, as concluded in Fig. 5, the free-electron regime is much more sensitive to electron-boundary scattering.

V. CONCLUSIONS

In this work, a reflectance model is developed that accounts for large temperature fluctuations in thin-film metals by utilizing the temperature dependencies of the intraband ("free" electron) and interband ("bound" electron) dielectric functions and multiple reflection theory. Electron-electron, electron-phonon, and electron-substrate (boundary) scattering are exploited and the change in reflectance as a function of these various scattering events is studied in the case of both intra- and interband excitations. This thermoreflectance model is compared to thermoreflectance data on thin Au films. The sensitivity of the thermoreflectance signal to electron-boundary scattering is discussed, and the thermoreflectance signal is much more sensitive to this electron-scattering mechanism in the free electron (intraband regime) than when approaching photon energies affected interband Fermi-surface transitions. This explains the discrepancy in electron-phonon coupling measurements observed in thin Au films.

ACKNOWLEDGMENTS

I am greatly appreciative for funding from the LDRD program office through Sandia National Laboratories. Sandia is a multiprogram laboratory operated by Sandia Corporation, a Lockheed-Martin Co., for the United States Department of Energy's National Nuclear Security Administration under Contract No. DE-AC04-94AL85000.

*pehopki@sandia.gov

[1] D. G. Cahill, Wayne K. Ford, Kenneth E. Goodson, Gerald D. Mahan, Arun Majumdar, Humphrey J. Maris, Roberto Merlin, and Simon R. Phillpot, J. Appl. Phys. **93**, 793 (2003).
[2] C. K. Sun, F. Vallee, L. Acioli, E. P. Ippen, and J. G. Fujimoto, Phys. Rev. B **48**, 12365 (1993).
[3] C. K. Sun, F. Vallee, L. H. Acioli, E. P. Ippen, and J. G. Fujimoto, Phys. Rev. B **50**, 15337 (1994).
[4] A. J. Sabbah and D. M. Riffe, Phys. Rev. B **66**, 165217 (2002).
[5] S. D. Brorson, A. Kazeroonian, J. S. Moodera, D. W. Face, T. K. Cheng, E. P. Ippen, M. S. Dresselhaus, and G. Dresselhaus, Phys. Rev. Lett. **64**, 2172 (1990).
[6] N. Del Fatti, C. Voisin, M. Achermann, S. Tzortzakis, D. Christofilos, and F. Vallee, Phys. Rev. B **61**, 16956 (2000).
[7] J. Hohlfeld, S.-S. Wellershoff, J. Güdde, U. Conrad, V. Jähnke, and E. Matthias, Chem. Phys. **251**, 237 (2000).
[8] P. E. Hopkins, J. L. Kassebaum, and P. M. Norris, J. Appl. Phys. **105**, 023710 (2009).
[9] P. E. Hopkins, J. M. Klopf, and P. M. Norris, Appl. Opt. **46**, 2076 (2007).
[10] P. E. Hopkins, Pamela M. Norris, Leslie M. Phinney, Steven A. Policastro, and Robert G. Kelly, J. Nanomater. **2008**, 418050.
[11] P. E. Hopkins and P. M. Norris, Appl. Surf. Sci. **253**, 6289 (2007).
[12] J. M. Klopf and P. M. Norris, Int. J. Thermophys. **26**, 127 (2005).
[13] J. M. Klopf and P. M. Norris, Appl. Surf. Sci. **253**, 6305 (2007).
[14] B. C. Gundrum, D. G. Cahill, and R. S. Averback, Phys. Rev. B **72**, 245426 (2005).
[15] B. M. Clemens, G. L. Eesley, and C. A. Paddock, Phys. Rev. B **37**, 1085 (1988).
[16] S. I. Anisimov, B. L. Kapeliovich, and T. L. Perel'man, Sov. Phys. JETP **39**, 375 (1974).
[17] A. N. Smith, J. L. Hostetler, and P. M. Norris, Numer. Heat Transfer, Part A **35**, 859 (1999).
[18] R. Rosei, Phys. Rev. B **10**, 474 (1974).
[19] R. Rosei, C. H. Culp, and J. H. Weaver, Phys. Rev. B **10**, 484 (1974).
[20] R. Rosei and D. W. Lynch, Phys. Rev. B **5**, 3883 (1972).
[21] W. J. Scouler, Phys. Rev. Lett. **18**, 445 (1967).
[22] J. Hanus, J. Feinleib, and W. J. Scouler, Phys. Rev. Lett. **19**, 16 (1967).
[23] E. Colavita, A. Franciosi, D. W. Lynch, G. Paolucci, and R. Rosei, Phys. Rev. B **27**, 1653 (1983).
[24] J. Hohlfeld, U. Conrad, J. G. Muller, S. S. Wellershoff, and E. Matthias, *Nonlinear Optics in Metals*, edited by K. H. Bennemann (Clarendon, Oxford, 1998), p. 219.
[25] J. Hohlfeld, D. Grosenick, U. Conrad, and E. Matthias, Appl. Phys. A: Mater. Sci. Process. **60**, 137 (1995).
[26] A. N. Smith and P. M. Norris, Appl. Phys. Lett. **78**, 1240 (2001).
[27] P. E. Hopkins, J. Appl. Phys. **105**, 093517 (2009).
[28] A. D. Rakic, Aleksandra B. Djurišic, Jovan M. Elazar, and Marian L. Majewski, Appl. Opt. **37**, 5271 (1998).
[29] E. D. Palik, *Handbook of Optical Constants of Solids* (Academic, Orlando, 1985).
[30] P. B. Johnson and R. W. Christy, Phys. Rev. B **6**, 4370 (1972).
[31] P. B. Johnson and R. W. Christy, Phys. Rev. B **9**, 5056 (1974).
[32] P. B. Johnson and R. W. Christy, Phys. Rev. B **11**, 1315 (1975).
[33] R. Hummel, *Electronic Properties of Materials* (Springer, New York, 2001).
[34] F. Abeles, in *Advanced Optical Techniques*, edited by A. C. S. V. Heel (North-Holland, Amsterdam, 1967), p. 145.
[35] H. A. Macleod, *Thin-Film Optical Filters* (Institute of Physics, Bristol, UK, 2001).
[36] S. S. Jha and C. S. Warke, Phys. Rev. **153**, 751 (1967).
[37] K. C. Rustagi, Nuovo Cimento B **53**, 346 (1968).
[38] J. M. Ziman, *Electrons and Phonons* (Clarendon, Oxford, 1960).
[39] N. E. Christensen and B. O. Seraphin, Phys. Rev. B **4**, 3321 (1971).
[40] M. Kaveh and N. Wiser, Adv. Phys. **33**, 257 (1984).
[41] X. Y. Wang, D. M. Riffe, Y. S. Lee, and M. C. Downer, Phys. Rev. B **50**, 8016 (1994).
[42] Z. Lin, L. V. Zhigilei, and V. Celli, Phys. Rev. B **77**, 075133 (2008).
[43] N. W. Ashcroft and N. D. Mermin, *Solid State Physics* (Saunders College, Fort Worth, 1976).
[44] A. Sergeev, B. S. Karasik, M. Gershenson, and V. Mitin, Physica B **316-317**, 328 (2002).
[45] A. V. Sergeev, Phys. Rev. B **58**, R10199 (1998).
[46] A. V. Sergeev, Physica B **263-264**, 217 (1999).